Bio-Design and Manufacturing (2019) 2:10–23
https://doi.org/10.1007/s42242-019-00035-w

RESEARCH ARTICLE

Three-dimensional VOF simulation of droplet impacting on a superhydrophobic surface

Jin Sun[1] · Qi Liu[1] · Yunhong Liang[2] · Zhaohua Lin[1,2] · Chunbao Liu[1,2]

Received: 6 January 2019 / Accepted: 30 January 2019 / Published online: 18 February 2019

Abstract

It is very important to analyze and study the motion process of droplets impacting superhydrophobic surface, which is of great significance to understand the mechanism of superhydrophobic surface and guide the design and manufacture of superhydrophobic surface. Taking by three-dimensional volume of fluid (VOF) simulation coupling coupled level set (CLS) algorithm, on the one hand, we simulate the morphological changes in the process of droplet impingement, as well as the internal velocity and the pressure distribution; on the other hand, we focus on the effects of droplet impact velocity, surface wettability, surface tension on the dynamics of the droplets. The CLSVOF model inherits the advantages of the VOF model for accurately constructing the phase interface and inherits the advantage that the level set can accurately calculate the surface tension, which improves the accuracy of the calculation of the droplet impact on the superhydrophobic surface. The computed results distinctly demonstrated there were four stages: falling, spreading, shrinking and rebounding. The time history of each stage agreed well with the pictures captured by high-speed camera, which indicated the computational fluid dynamics scheme was effective. Moreover, the motion mechanism of the droplets impacting on the solid surface is elaborated, which was helpful to control the solid–liquid interface to achieve a variety of solid interface characteristics.

Keywords Superhydrophobic · Droplet impact · Computational fluid dynamic · VOF

Introduction

From the initial "lotus leaf effect" to rice leaf, taro leaf, rose petal, cicada's wing, water strider leg and mosquito eye with the same superhydrophobic effect, different kinds of superhydrophobic biological samples have been found continuously. According to its special important characteristics such as waterproof, antifouling, anticorrosion and self-cleaning, superhydrophobic technology can be applied to many fields such as construction industry, pipeline transportation, medical–health care profession, national defense and military affairs.

Inspired by the superhydrophobic phenomena in nature, researchers designed and fabricated biomimetic superhydrophobic surfaces to disturb the flow behavior of liquid–solid surfaces with the purpose of reducing the flow loss of solid wall surface. Study on the flow behavior of superhydrophobic surface droplets will provide a theoretical basis for bionic design.

In the field of mechanical science, materials science, chemical engineering and others, there are usually droplets impacting on the solid surface, such as the oil spray in diesel engines and the droplets splashing on the surface of containers in chemical industry manufacturing [1–3]. In order to avoid the crushing phenomenon and energy loss caused by impact, researchers have conducted a lot of research on the dynamic characteristics of droplets [4–6]. In recent years, the dynamic characteristics of the droplets impacting on the hydrophobic or superhydrophobic surface have attracted an increasing attention [7–10].

Electronic supplementary material The online version of this article (https://doi.org/10.1007/s42242-019-00035-w) contains supplementary material, which is available to authorized users.

✉ Zhaohua Lin
linzhaohua@jlu.edu.cn

✉ Chunbao Liu
liuchunbao@jlu.edu.cn

[1] School of Mechanical Science and Aerospace Engineering, Jilin University, Changchun 13002, China

[2] Key Laboratory of Bionic Engineering, Ministry of Education, Jilin University, Changchun, China

There are three methods for the research on the phenomenon of droplets impacting on the solid surface: theoretical study, numerical simulation and experimental investigation. In the field of theoretical research, Vafaei et al. [11, 12] have studied the influence of the geometrical size of droplets on the contact angle. Under the assumption that the interaction between gravity and surface tension was ignored, the force analysis of the droplets was performed and a mathematical model was established; thus, the theoretical relation that physical property parameter, quality and other parameters were given to solve the size of the contact angle was obtained. Zhang [13] and others have studied the impact behavior between the supercooled droplets and various superhydrophobic surfaces; also the dynamic effects of roughness, temperature and wettability on the impact of supercooled droplets were discussed. In the field of numerical simulation, Shin et al. [14, 15] and others have used the horizontal contour reconstruction (LCRM) method to numerically analyze the impact of droplets on periphery with superhydrophobic characteristics. Through the analysis, it was found that while the impact velocity was low, the contact time between the droplets and the surface rapidly decreased as the impact velocity went up, yet while the impact velocity is high, the change in contact time was negligible. In the field of experimental research, the relationship between the critical impact velocity of the droplets impacting on the superhydrophobic surface and the geometric structure of the impact surface was studied through experiments by Hao et al. [16]. It was shown that the roughness and microstructure of the impact surface would produce high liquid pressure on the droplets [17–19].

In this paper, the dynamic process and energy distribution of the droplets impacting on a superhydrophobic surface are numerically simulated by three-dimensional VOF simulations coupling CLS algorithm. We aim to capture and analyze the dynamic process of the droplets impacting on superhydrophobic surface, which contributes to understand the multiphase flow mechanism in the solid–liquid interface. Through the in-depth analysis on the droplet impact process and the morphological changes, the paper offers theoretical reference for the related fields involving droplets impacting on the superhydrophobic surface.

The coupling of the level set and the VOF (CLSVOF) overcomes the disadvantages of inaccuracy in the process of the VOF calculating the parameters such as normal direction and curvature; also it ensures the mass conservation of the level set in the process of ϕ function convection transport and reinitialization, which makes capture of the phase interface more accurate and sharp [20, 21]. The basic computational flow calculated by the coupling of the two methods is shown in Fig. 1.

Computational scheme

Computational model

The physical model of the droplets impacting on the superhydrophobic surface is shown in Fig. 2a; the droplets with a certain initial velocity vertically impact onto the superhydrophobic surface. In the motion process, the droplets are influenced by the gravity $g = 9.81$ kg/m^2; the direction is vertically downward. Figure 2b shows a computational domain geometry model for numerical simulation, which is a three-dimensional cylinder with a bottom diameter of $D = 10$ mm and a height of $h = 6$ mm.

The study of the droplets impacting on the surface refers to the two-phase flow of the two media: liquid phase (water) and gas phase (air). In the CFD calculation, the coupling of the volume of fluid (VOF model) and the level set method is used to track the interface position of the two phases, in which the air is the main phase and the water is the secondary phase. The specific material parameters are shown in Table 1.

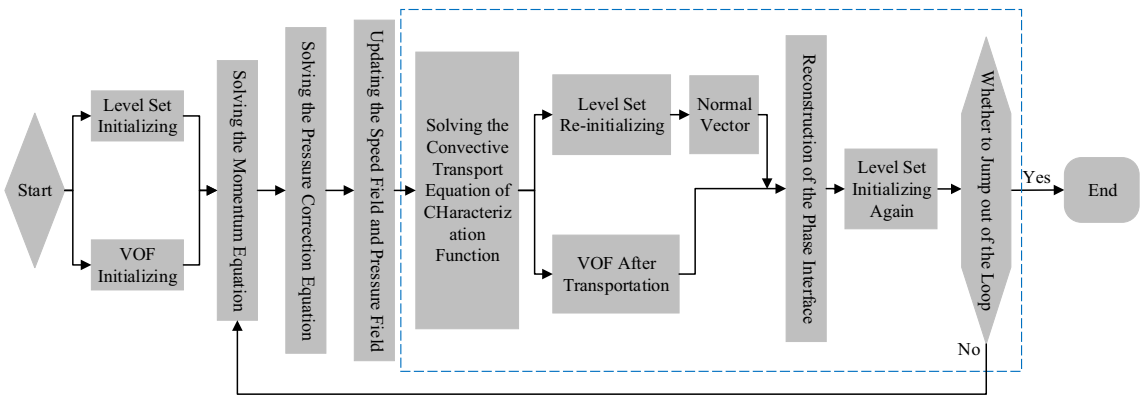

Fig. 1 Computational flow diagram of level set VOF (CLSVOF)

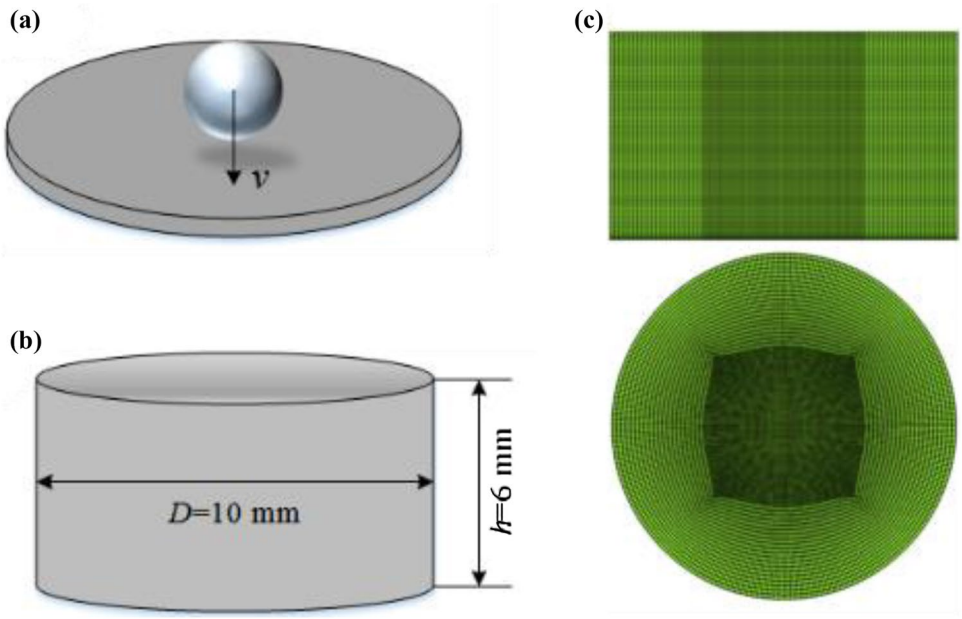

Fig. 2 The physical model and computational domain model of the droplets impacting on the solid surface. **a** The physical model that the droplets hit the superhydrophobic surface at a velocity perpendicular to the superhydrophobic surface. **b** A cylindrical numerical simulation domain ($D=10$ mm, $h=6$ mm). **c** The drawn grid of numerical simulation

Table 1 Material parameters of two-phase media

Media	Main phase Air	Secondary phase Water
Density	1.225 kg/m^3	998.2 kg/m^3
Viscosity	1.7894×10^{-5} Pa/s^{-1}	0.001003 Pa/s^{-1}
Surface tension coefficient	0.073 N/m	

In the solution process, the air is the main phase, the water is the secondary phase, and the pressure-based implicit algorithm is used to process the transient solution of the impacting process of the droplets. In the falling process, the droplets are driven by gravity, and the gravitational acceleration is $g=9.81$ kg/m^2, which is vertically downward along the z-axis of the coordinate system. The lower boundary of the computational model area is set as a superhydrophobic nonslip surface, and the rest of the boundary is set as the pressure outlet boundary, with the pressure of 0. The PISO algorithm is used for the coupling of the pressure–velocity, in which the gradient format is Least Squares Cell Based, the pressure difference format is PRESTO, the volume fraction is solved by Geo-Reconstruct and the second-order upwind format is adopted in other spatial discretization. The sub-relaxation factor is in default value——pressure of 0.3, density of 1, body force of 1 and torque of 0.7. After global initialization, a water droplet with the initial velocity in downward motion is defined in the computational field through the adapt and patch functions. The calculation of CFD can be performed automatically by setting the appropriate time step and the number of time steps.

Since the structure of this computational model is relatively simple and small in size, the ICEM (The Integrated Computer Engineering and Manufacturing) software is used for the hexahedral structure grid. The central region of the cylindrical computational field is the main region of the droplet motion, and the bottom surface area is the area where the droplets interact with the solid surface, so grid encryption is performed in these two parts to improve the accuracy of the numerical calculation. The gird is shown in Fig. 2c. The cell number is 1.6 million. Based on the above factors and the numerical computing results of a droplet with a diameter of 1.6 mm at an initial velocity of $v=0.45$ m/s vertically impacting on a superhydrophobic solid surface with a contact angle of $\theta=152.4°$.

Computational validation

It is a dynamic process that the motion of droplets impacts on the solid surface, in which the shape of the droplets constantly changes. In order to quantitatively study the motion process of the droplets, three-dimensional parameters are defined according to Fig. 3: spreading coefficient β, compressing/stretching coefficient δ and rebound coefficient λ. The function definition is as follows:

$$\beta=\frac{D}{D_0} \tag{1}$$

$$\delta=\frac{h_2}{D_0} \tag{2}$$

$$\lambda=\frac{h_1}{h_0} \tag{3}$$

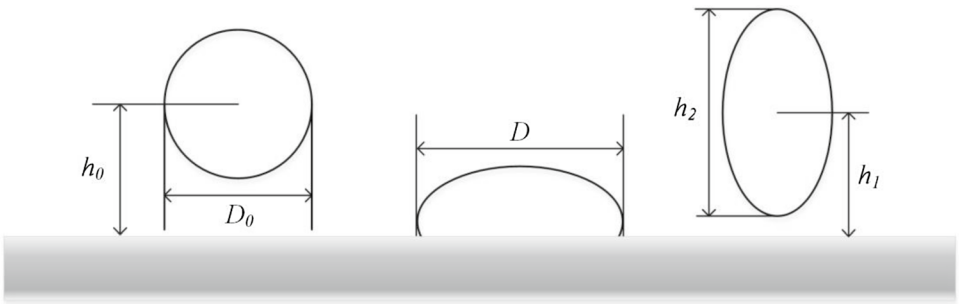

Fig. 3 The shape parameters of the droplets

In the equation, D_0—the initial diameter of the droplets (mm), D—the spreading diameter of the droplets (mm), h_0—the initial dripping height of the droplets (mm), h_1—the maximum rebound height of the droplets (mm), h_2—the thickness of the droplets compressing/stretching (mm).

Captured by a high-speed camera, Fig. 4a shows the motion state [1, 12] of the droplet at the diameter of 1.6 mm at different moments after it impacts on the superhydrophobic with the speed of $v = 0.45$ m/s. Figure 4b shows the numerical calculation of the motion state after the droplets impacting on the superhydrophobic surface under the same initial conditions. It can be clearly seen from the comparison chart that the numerical simulation motion of the droplets and the motion of the droplets captured in the experiment are basically consistent in the time node and the motion morphology, which shows that it is feasible to simulate the motion state of droplets impacting on the superhydrophobic surface by numerical calculation, and the calculation results can be used to further analyze the interaction between the droplets and the superhydrophobic surface.

The experimental test data and numerical calculation data of the spreading coefficient in the processing of the droplet impacting on the superhydrophobic surface are extracted, and the comparison diagram shown in Fig. 5a is drawn. It can be seen from the diagram that the numerical simulation results of the spreading coefficient are in good agreement with the experimental test results. The spreading coefficient increases sharply first and then decreases rapidly. The droplets at around 6.8 ms depart from the solid surface, and the spreading coefficient drops to 0. Figure 5b shows the contrast error value between the numerical simulation results of the spreading factor and the experimental test results at each time node in the first 5 ms. The error value between the numerical results and the experimental results within the first 5 ms is less than 15%, and the error value is within the acceptable range, especially in the first 3 ms, the error value is less than 10%, and the degree of coincidence in contrast is very high. After 5 ms, the droplets are in the late stage of retraction. The error value at this time is relatively large, but the overall trend of the spreading coefficient curve is consistent. Considering the presence of measurement error

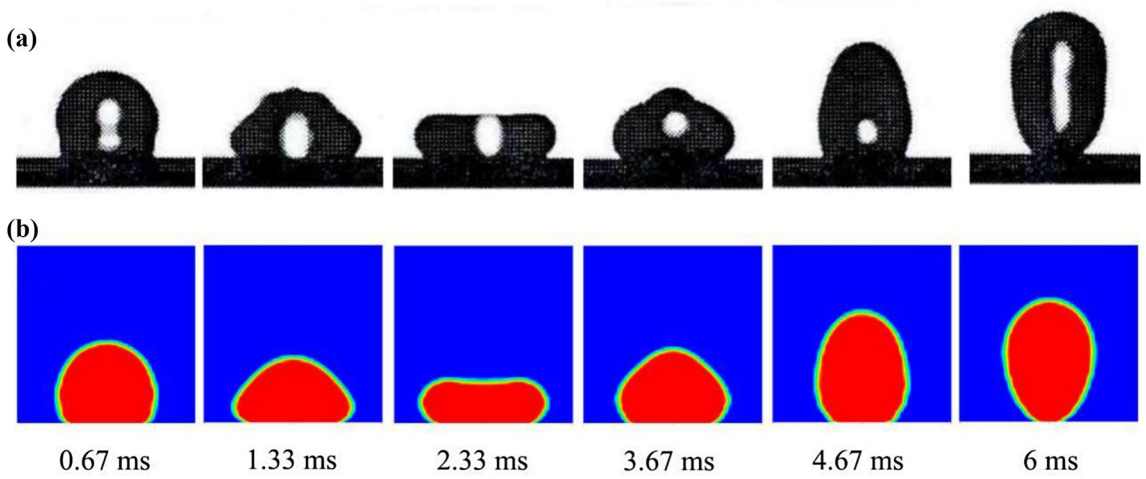

Fig. 4 The experimental results and numerical calculations of the droplets impacting on the superhydrophobic surface. **a** Captured by a high-speed camera, the motion state of the droplet at the diameter of 1.6 mm at different moments after it impacting on the superhydrophobic with the speed of $v = 0.45$ m/s. **b** The numerical calculation of the motion state after the droplets impacting on the superhydrophobic surface under the same initial conditions

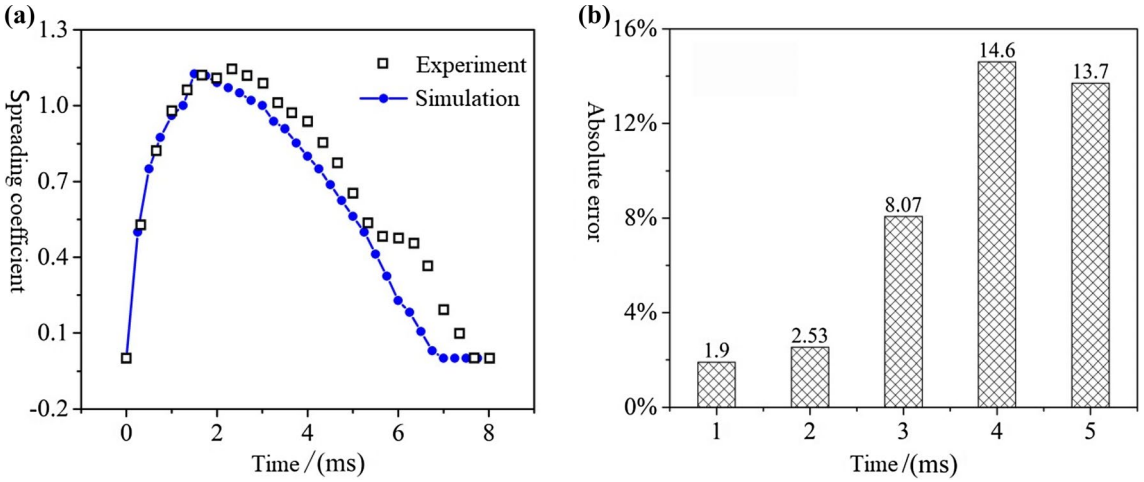

Fig. 5 The variation law of spreading coefficient and error analysis of simulation and experimental results. **a** The comparison diagram of experimental test data and numerical calculation data of the spreading coefficient in the processing of the droplet impacting on the superhydrophobic surface. **b** The contrast error value between the numerical simulation results of the spreading factor and the experimental test results at each time node in the first 5 ms

and human factors, it is still possible to use the compound level set VOF method to trace gas–liquid two-phase flow interface in the moving process of the droplets impacting on the solid surface.

Results

3D morphology

In order to accurately analyze the changes of the motion morphology of the droplets after impacting on the superhydrophobic solid surface, as well as to obtain a more obvious impacting effect, the numerical simulation for the droplets at a diameter of 2 mm impacting on the superhydrophobic with a $\theta = 160°$ contact angle at an initial velocity $v = 1$ m/s is performed. Figure 6 shows the simulation of the three-dimensional shape of the droplet motion at different moments and the two-dimensional shape of the YZ section.

After the droplets impacting on the solid surface, four processes of spreading, retracting, rebounding and falling are cyclically performed until the energy is dissipated, and static on the solid surface remains in a certain form. In the spreading stage, due to the difference in the dynamic distribution of the fluid inside the droplets, the droplets gradually spread from the center to the periphery, and the contact area between the droplet and the surface reaches the maximum at about 2 ms (Fig. 6b). At this time, the center height of the droplet is basically consistent with the height of the edge, and the two parts are transitioned in an inset circular arc with large curvature. After that, the liquid in the center of the droplet continues to move downwards while the liquid in the extrusion center flows to the edge. The edge of the droplet can no longer be spread due to the surface tension, so the liquid accumulates in the edge region and finally forms a concave, in which the periphery is high yet the center is low (Figure 6d).

When the central liquid reaches the lowest position, the droplet formally enters the stage of retraction and rebound. Under the action of surface tension, the outer ring liquid shrinks and extrudes inward causing the liquid in the center area rebounds, and the contact area between the liquid and the solid surface gradually decreases. The liquid at the center is squeezed to move upward at a great velocity, while the liquid at the bottom moves inward at a transverse velocity, so that the upper liquid moves a greater axial distance than the lower liquid per unit time. The droplet starts to rebound in a shape of "gourd," in which the upside is narrow, yet the bottom is wide (Fig. 6e–i), until finally leaving the solid surface.

Due to the difference in the velocity distribution inside the droplet, the upper liquid will reach the highest position of the rebound earlier than the lower liquid. As time progresses, the liquid in the lower area will gradually reach the highest position, so the motion morphology will appear as the shape of an "inverted pear" the upside is wide, yet the bottom is narrow. When the droplet rebounds to the highest position, the droplet begins to fall again under the action of gravity, and repeat all stages of the previous cycle until the energy is depleted to rest on the solid surface.

The outer contour of the droplet was drawn through the four typical moments in the process of rebound, as shown in Fig. 7a. It can be clearly seen from the diagram that with the progress of the contraction and rebound of the droplet, the edge of the droplet shrinks inward under the action

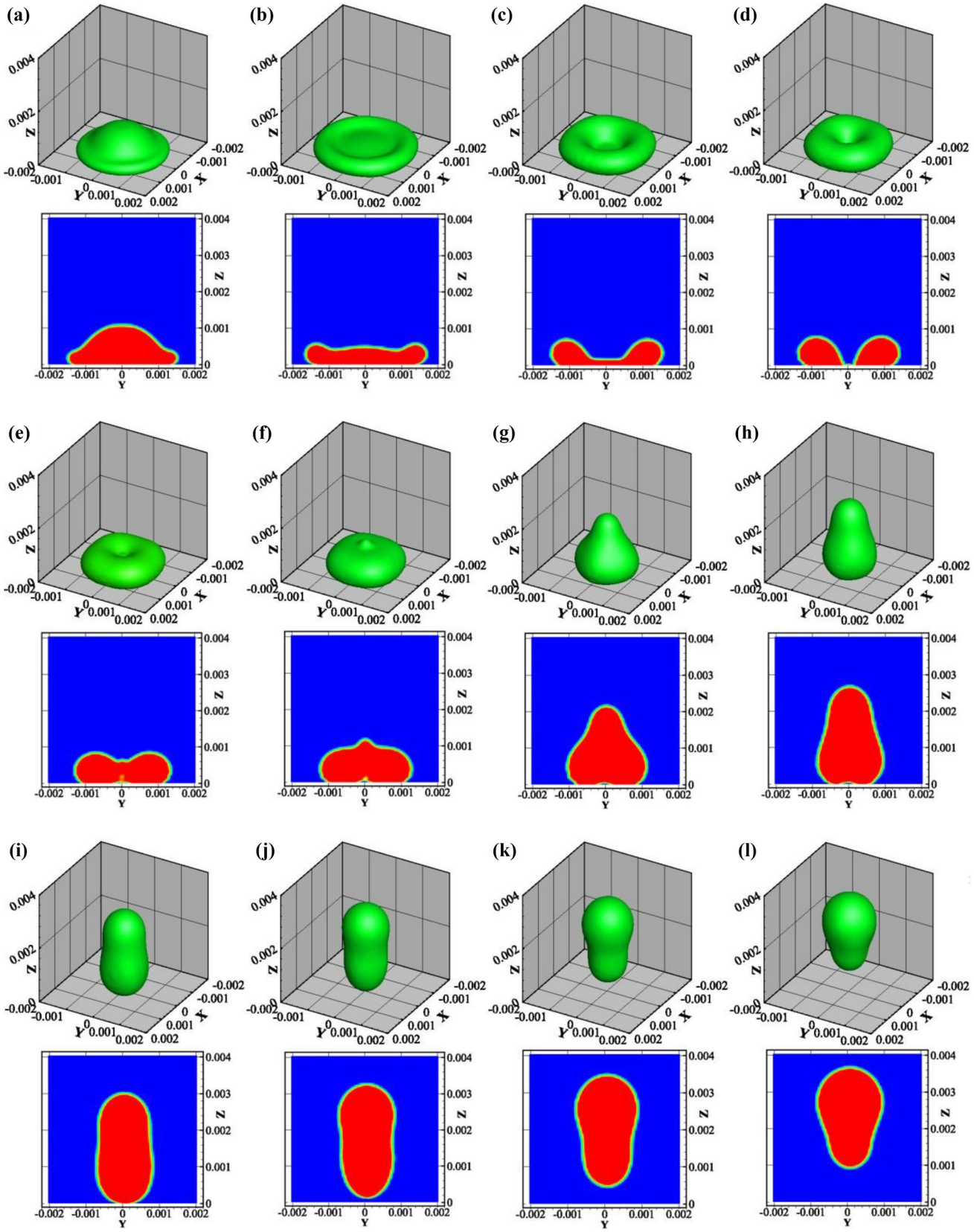
(a)
(b)
(c)
(d)
(e)
(f)
(g)
(h)
(i)
(j)
(k)
(l)
Z
X
Y
0.004
0.002
-0.002
-0.001
0
0.001
0.002
0.003

◂**Fig. 6** The motion morphology of the droplet in different moments. The simulation of the three-dimensional shape of the droplet motion at different moments and the two-dimensional shape of the YZ section. **b** The maximum of the contact area between the droplet and the surface at about 2 ms. **d** The droplet with the shape of concave. **e–i** The motion morphology of the droplet rebounding in a shape of "gourd," which the upside is narrow yet the bottom is wide

of surface tension, which drives the center liquid to move upward at the same time. From Fig. 7b, it can be found that in the process of rebound, the droplet is not clinging to the solid surface, but forms a concave "air cavity" at the position where the droplet axis contacts with the surface. This "air cavity" decreases as the contact area decreases (the area between the droplet and the solid surface), and disappears at a certain contact diameter. It can be known from the analysis that the liquid on the drop axis has a vertical upward velocity, while the liquid far from the axis is an oblique upward velocity vector. The velocity vector can be decomposed into a lateral velocity directing toward the axis and an upward longitudinal velocity paralleling to the axis. The droplet contracts because of the transverse velocity, while the droplet moves upwards due to the longitudinal velocity. In the axial direction, the liquid in the center position has a greater axial velocity than the liquid at the edge position, so that the liquid in the central region has a larger moving distance per unit time. Thus, the bottom surface of the droplet forms a concave "air cavity" by the presence of the velocity difference.

Figure 8 shows a graph showing the spreading coefficient and the compressing coefficient changing over time after the droplet contacts with the solid surface. As shown in Fig. 8a, the spreading coefficient shows a tendency to increase first and then decrease. At the initial stage, the droplet has a large initial velocity and spreads rapidly on the solid surface after contacting with the solid surface, which shows in the graph that the spreading coefficient increases sharply. At around 2 ms, the spreading coefficient reaches the maximum value, about 1.4. In the stage of spreading, the kinetic energy and the gravitational potential energy of the droplet are mostly converted into the surface energy, while the remainder is used to overcome the viscous work and frictional work of the solid surface. Between 1.5 ms and 2.5 ms, the spreading coefficient changes relatively slowly. This is because when the droplet reaches or is about to reach the maximum spreading state, the motion of the internal mass of the droplet is homogenized, so that the diameter of the contact circle of the droplet with the surface changes little. Then the droplet quickly retracts and the spreading coefficient sharply decreases with a large amplitude until the droplet rebounds away from the solid surface after 8 ms. In the stage of retracting, the surface energy of the droplet is converted into the kinetic energy and the gravitational potential energy again, but there is still a part of energy loss to overcome the viscous work and frictional work of the solid surface. At this stage, due to the accumulation of energy loss, the retraction time of the droplet is prolonged and the variation trend of the spreading coefficient is slower than the spreading stage. Referring to Fig. 8b, when the droplet reaches the maximum spread state, the liquid in the center of the droplet is still at a downward velocity, so that the center liquid continues to move downward to compress the droplet. At about 3.6 ms, the droplet reaches its maximum compression state, at which point the center liquid velocity is zero, but there is still a large upward acceleration. Thereafter, the center of the droplet begins to move upwards under the action of acceleration, which is shown in the graph that the compressing coefficient increases sharply. At around 8 ms, the compression coefficient is up to a maximum of approximately 1.59. At this point, the droplet is in the maximum tensile state, and the

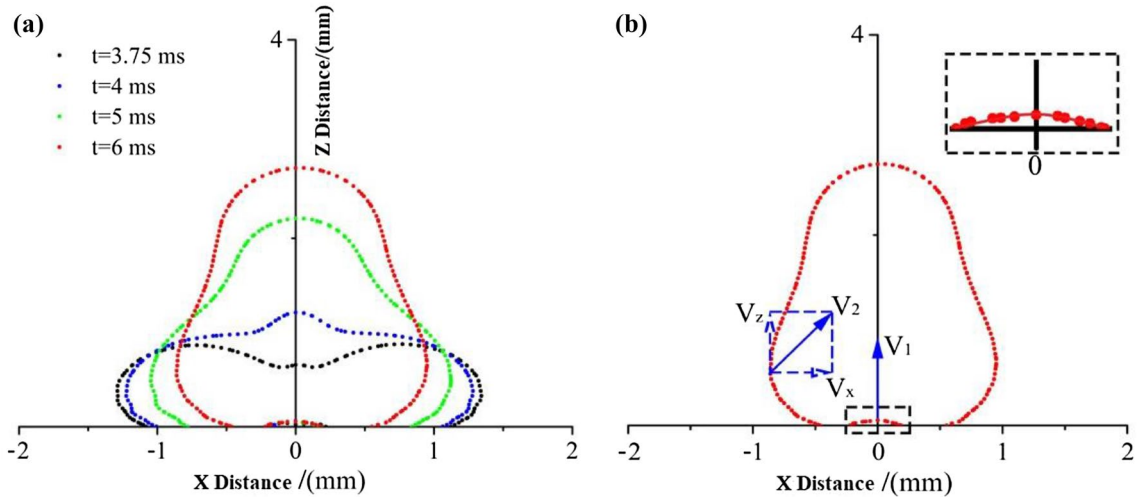

Fig. 7 Contour curve of the droplet at typical moment. **a** The outer contour of the droplet at the four typical moments in the process of rebound. **b** A concave "air cavity" at the position where the droplet axis contacts with the surface in the process of rebound

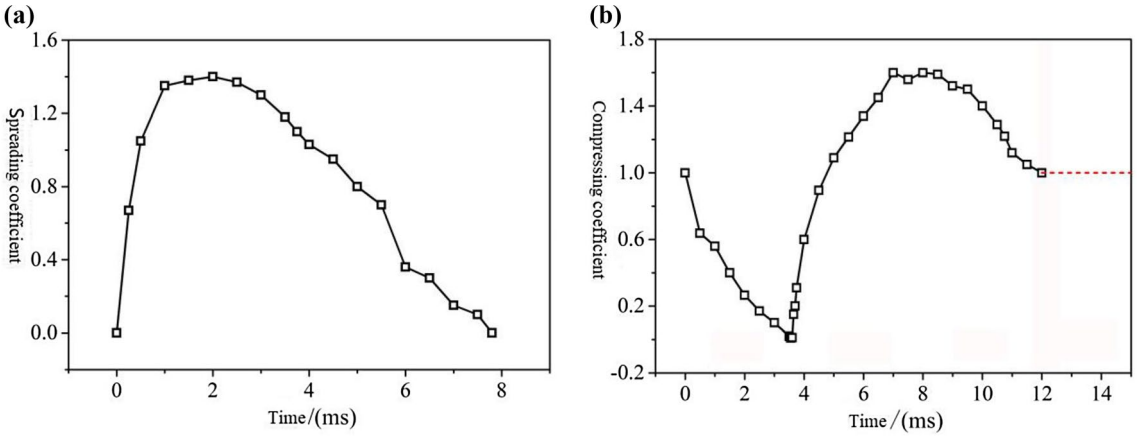

Fig. 8 The graph of the spreading coefficient and the compressing coefficient that changing over time. **a** The curve of spreading coefficient of droplet over time after the droplet contacts with the solid surface. **b** The curve of compressing coefficient of droplet over time after the droplet contacts with the solid surface

liquid velocity in the upper portion of the droplet is equal to the liquid velocity in the lower portion. The droplet then leaves the surface and enters the rebound stage, at which the overall velocity of the droplet gradually decreases. However, the velocity decrease in the lower liquid is smaller in amplitude than the velocity decrease in the upper liquid. The droplet as a whole shows a compressed state. Until the highest position is reached, the overall velocity of the droplet drops to zero, at which point the kinetic energy of the droplet is converted into gravitational potential energy except for a small portion of the energy loss.

Figure 9 shows the situation changes of the rebound coefficient and contact time of the droplets at different impact velocities. It can be clearly seen from the diagram that as the impact velocity increases, the rebound coefficient of the droplet gradually decreases, yet the contact time gradually increases. After analysis, it can be known that when the impact velocity is small, the contact time between the droplet and the solid surface is short, and the energy loss when the droplet spreads on the surface is relatively small, so the rebound coefficient of the droplet is large. With the increase in impact velocity, the contact time between droplet and surface is increased, and the energy loss of the droplet on the surface increases correspondingly, and the air resistance in the process of rebound also increases. Under the comprehensive action, the rebound coefficient of the droplet gradually decreases. If the impact velocity of the droplet continually increases, the droplet will break.

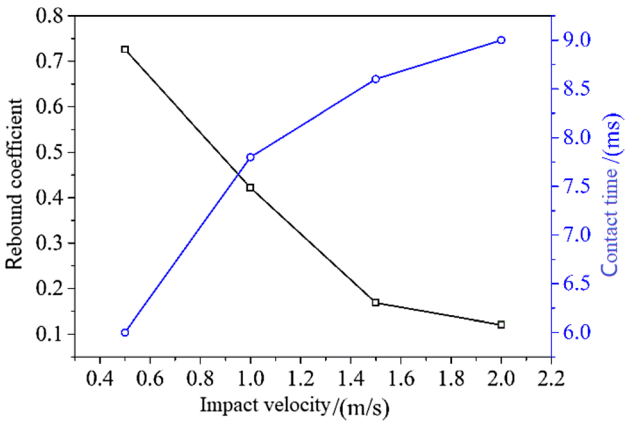

Fig. 9 The rebound coefficient and contact time of the droplets at different impact velocities

Flow field

Figure 10 shows the internal velocity cloud diagram and vector changes of the droplet impacting on the surface at different times. At the moment when the droplet impacts on the solid surface, the velocity of the liquid near the surface decreases sharply; especially, where near the central axis of the surface contact area, the liquid velocity is close to zero. The liquid velocity in the upper part of the droplet is relatively large due to the buffering of the motion. Figure 10a shows that the internal velocity of the droplet is distributed in an arc-like hierarchy, the outer liquid velocity is large, and the inner liquid velocity is small. In the stage of spreading, the upper liquid moves downward with a larger longitudinal velocity to push the edge of the liquid to the periphery, making the liquid that near the surface produce a large transverse velocity. As the droplet spreads over the surface, the lateral velocity at the edge of the droplet gradually decreases. When the thickness at the edge of the droplet coincides with that at the center, the velocity of the edge decreases to zero, at which point the spreading diameter of the droplet also reaches the maximum. Thereafter, the liquid in the

center of the droplet continues to move downward under the action of inertia, and the liquid at the edge is subjected to the extrusion and the surface tension of the liquid in the central region to produce an obliquely upward velocity; thus, the liquid accumulates at the edge (Fig. 10b, c). When the thickness of the liquid on the central axis is at the minimum, the liquid enters the contraction stage completely. At this stage, the edge of the droplet rebounds inwardly with an obliquely upward velocity vector, and the liquid at the central axis moves upward at a vertical upward velocity. It can be clearly seen from the cloud diagram that in the stage of rebound, the upper axis of the liquid has a large rebound velocity, which forms a gourd-like "air cavity" at the surface in the motion morphology. In the whole spreading and contracting stage, the contact area of the droplet with the surface is the position where the overall velocity of the droplet is at a minimum. Figure 10d–h shows that the maximum velocity of the droplet gradually moves downwards from upwards and appears at the bottom at the final stage, which also causes the compressed form of the droplet in the process of rebound, namely, the shape of "inverted pear" mentioned above.

Figure 11 shows the velocity distribution curve of the largest section of the droplet in the spreading state ($t=2$ ms). As shown in Fig. 11a, the liquid velocity is zero at the central axis. The liquid on both sides of the central axis has a velocity of moving toward the two sides, respectively. Within 0.8 mm from the central axis, the lateral velocity of the droplet gradually increases and reaches a maximum at 0.8 mm. At 0.8 mm to the edge of the droplet, the lateral velocity decreases until to zero at the edge. Referring to Fig. 13b, the longitudinal velocity of the liquid is large at the central axis, indicating that the liquid at this position moves vertically downward. In the interval of −0.8 mm to 0.8 mm, the liquid has a downward longitudinal velocity, indicating that the liquid in this interval still moves downward, while the liquid outside this interval is driven upward by the squeeze of the central droplet. There is a large longitudinal velocity at the edge of the droplet, but the lateral velocity is 0, indicating that the liquid at edge moves upward.

Figure 12 shows the velocity distribution curve of the droplet circular section with the maximum diameter when the droplet is retracted ($t=6$ ms). As shown in Fig. 14a, the internal velocity of the droplet is symmetrically distributed along the central axis. The velocity in the center is zero and the maximum velocity appears at the edge. According to the velocity distribution law, it can be known that the liquid on this section all contracts inwardly. Figure 12b shows the distribution trend of liquid longitudinal velocity on the

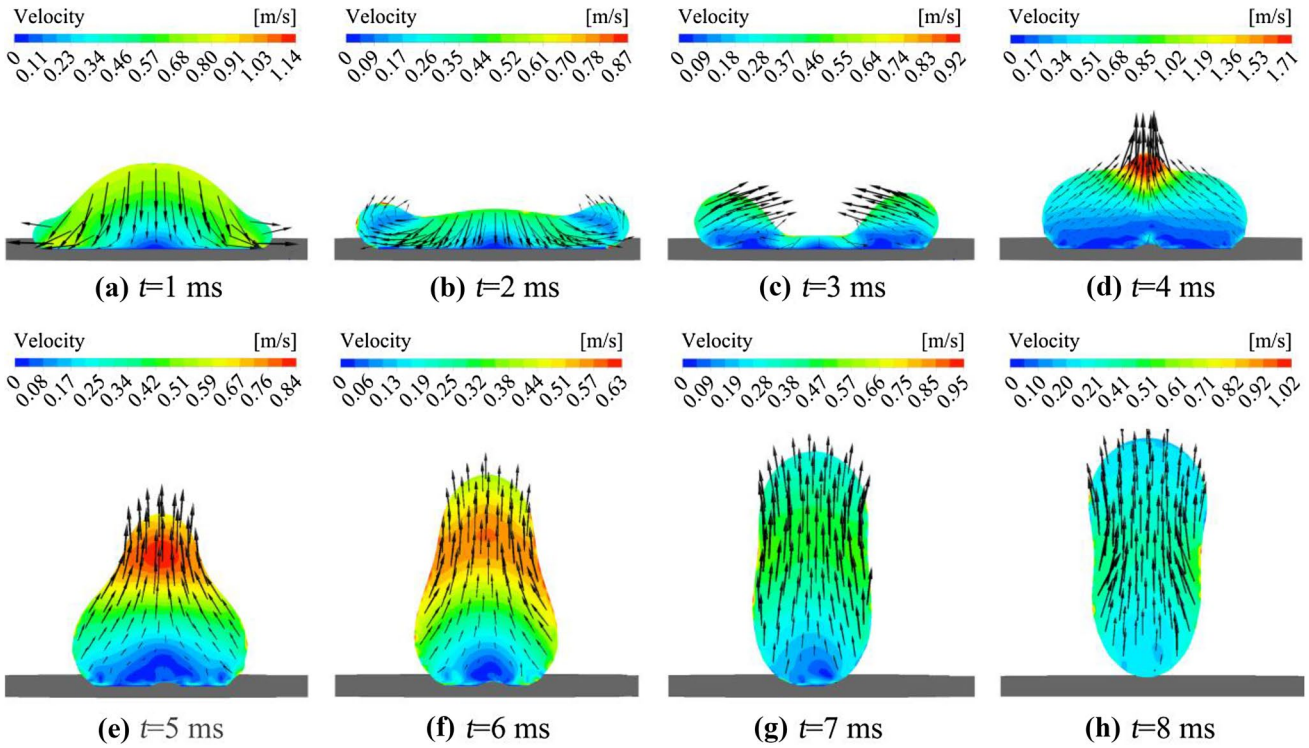

Fig. 10 Velocity cloud diagram and vector changes when the droplet impacting on the surface. **a** The internal velocity of the droplet is distributed in an arc-like hierarchy, the outer liquid velocity is large, and the inner liquid velocity is small. **b**, **c** The liquid in the center of the droplet continues to move downward under the action of inertia, and the liquid at the edge is subjected to the extrusion and the surface tension of the liquid in the central region to produce an obliquely upward velocity; thus, the liquid accumulates at the edge. **d**–**h** The maximum velocity of the droplet gradually moves downwards from upwards and appears at the bottom at the final stage

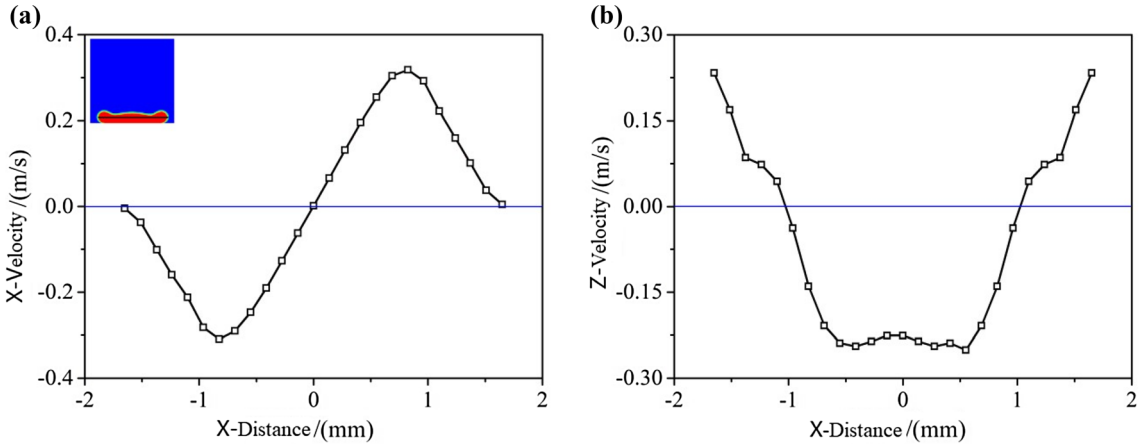

Fig. 11 Velocity distribution curve of the droplet section at $t=2$ ms. **a** The X-velocity distribution curve of the largest section of the droplet in the spreading state ($t=2$ ms). **b** The Z-velocity distribution curve of the largest section of the droplet in the spreading state ($t=2$ ms)

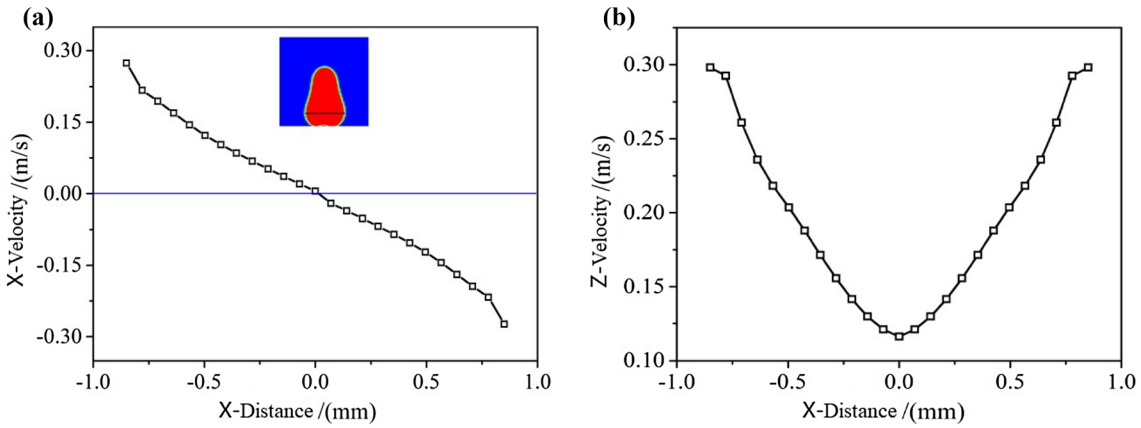

Fig. 12 Velocity distribution curve of the droplet section at $t=6$ ms. **a** The X-velocity distribution curve of the largest section of the droplet in the spreading state ($t=6$ ms). **b** The Z-velocity distribution curve of the largest section of the droplet in the spreading state ($t=6$ ms)

interface. It can be found that the longitudinal velocity values of the liquid on the cross section are all greater than zero, indicating that the liquid at this time is all moving upward. At the same time, the central longitudinal velocity is the smallest, while the longitudinal velocity of the edge area is the largest. Referring to Fig. 12a, b, the liquid at the edge moves at an obliquely upward velocity, and the liquid in the center area only has a velocity to move vertically upward, which results in the "air chamber" in Fig. 7.

Figure 13 shows the pressure distribution cloud diagram inside the droplet at different times. At the moment when the droplet contacts the surface, the pressure in the liquid region near the surface instantaneously increases; thus, a large range of high-pressure zone is produced. As the droplet spreads over the surface, the pressure at the edge area increases, yet the internal pressure gradually decreases. In the arc area where the outer ring transits to the central part, a negative pressure is generated by the change in the direction of the liquid velocity in this area. From the overall pressure distribution, the internal pressure of the droplet is axially symmetrical distribution. When the droplet reaches the maximum spreading state around $t=2$ ms, there are two high-pressure zones symmetrically distributed at the edge. Thereafter, the high-pressure zone moves inward and gradually moves upward as the droplet rebounds. During the movement of the high-pressure zone, it separates into the top and bottom directions, respectively, thus forming the upper and lower two high-pressure zones. It can be clearly seen from the figure that in the rebound process of the droplet, the upper and lower high-pressure zones are always exist, which also causes the droplet to rise in the form of constant retracting–stretching fluctuations in the rebound process.

Figure 14 shows the pressure variation curve of the solid surface in the process of the droplet impacting on it. It can be clearly seen from the graph that there are three peaks

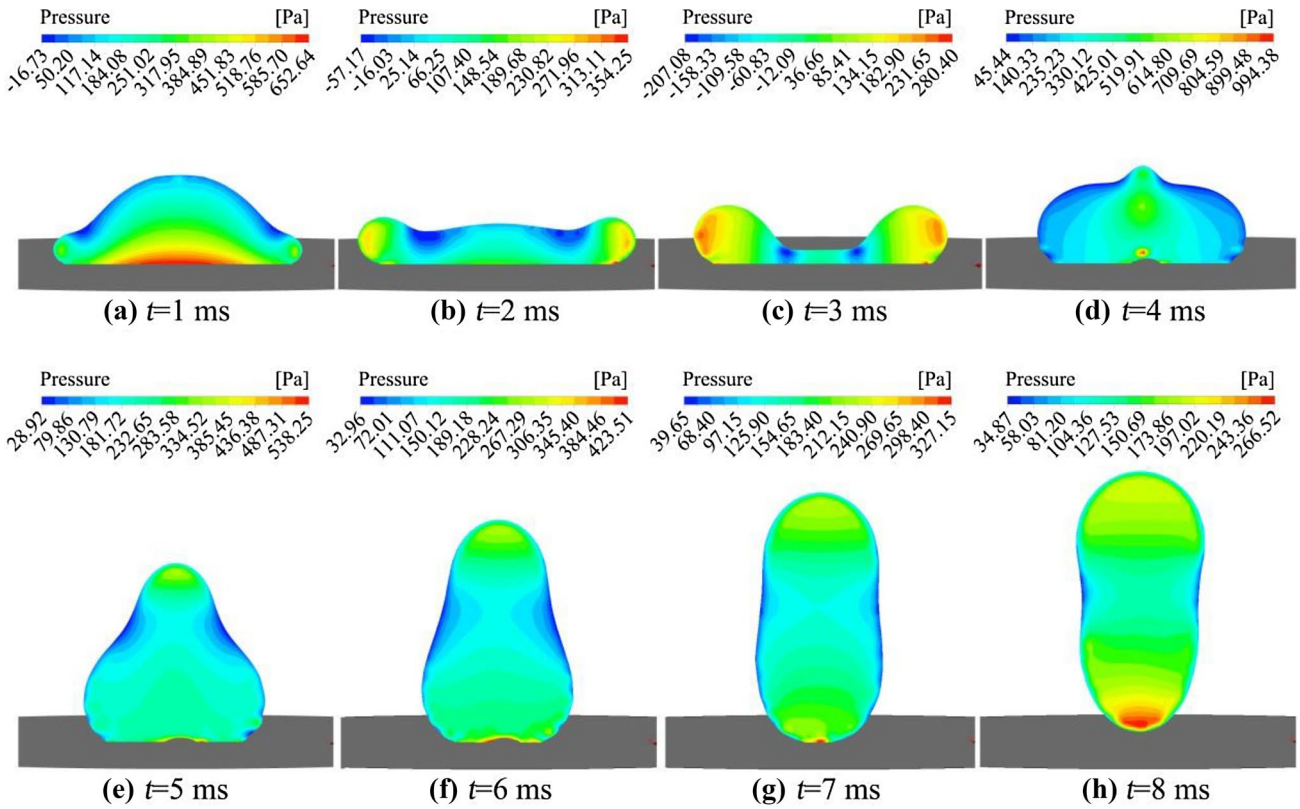

Fig. 13 Cloud diagram of pressure distribution at different times

in the pressure value, which are 0.02778 Pa, 0.00392 Pa and 0.00227 Pa, respectively. The three peaks appear at the moment of impacting, the spreading factor of 1 and minimum compression state, respectively. At the moment of impacting, the pressure on the surface instantly reaches a maximum and then quickly drops to the lowest point. As the droplet comes into contact with the surface, there will be an amplification interval in the pressure on the surface. When the spreading diameter is the same as the droplet diameter, the pressure on the surface reaches the second peak of wave. Thereafter, the pressure on the surface slowly decreases as the droplet spreads over the solid surface. When the liquid at the droplet axis is compressed to the lowest point, the pressure on the surface instantaneously rebounds to the third peak of wave, and then, the pressure gradually decreases until the droplet leaves the surface and drops to zero.

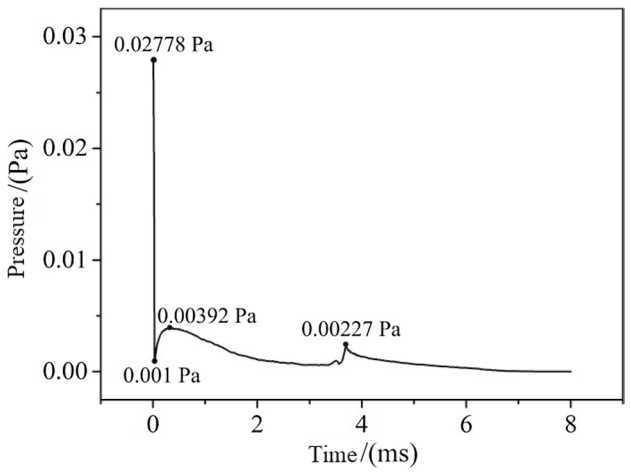

Fig. 14 The pressure variation curve of the surface. The pressure variation curve of the solid surface in the process of the droplet impacting on it with three peaks in the pressure value, which are 0.02778 Pa, 0.00392 Pa and 0.00227 Pa, respectively

Figure 15 shows the analysis of the pressure values on the circular section of the maximum spreading diameter of the droplet at $t=2$ ms and $t=6$ ms, respectively. Figure 15a shows that the internal pressure of the droplet is axially symmetrical distributed and there is a large pressure distribution at the edge. While $x=-0.8$ mm and $x=0.8$ mm, the droplet pressure is less than zero for negative pressure, which indicates that the internal velocity of the droplet changes significantly at this position. At the center of the droplet, there is a relatively large positive pressure on it, indicating that it still has a trend to move downward. Figure 15b shows that the internal movement tendency of the droplet is uniform. It is also inferred from the pressure distribution

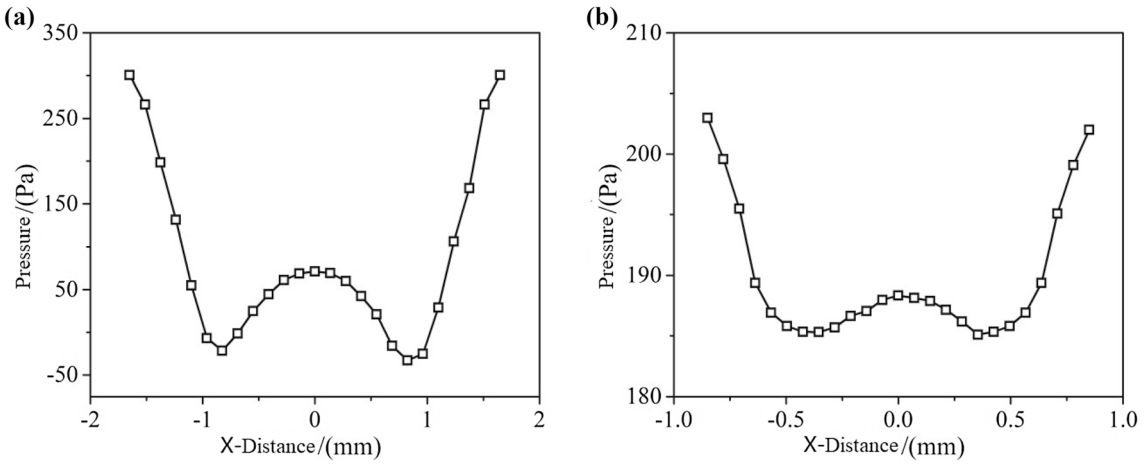

Fig. 15 Pressure distribution inside the droplet at different times. **a** The analysis of the pressure values on the circular section of the maximum spreading diameter of the droplet at $t = 2$ ms. **b** The analysis of the pressure values on the circular section of the maximum spreading diameter of the droplet at $t = 6$ ms

curve that the velocity within the droplet is distributed in arc-like hierarchy.

Crushing behavior

Captured by a high-speed camera, Fig. 16 shows the crushing pattern of a 2-mm-diameter droplet at a preliminary velocity of $v = 1$ m/s impacting on a hydrophobic surface with a contact angle of $\theta = 160°$ [22]. It can be seen from the diagram that the crushing of the droplet can be divided into two stages. At the stage of spreading, the surface tension of the droplet edge cannot maintain the rapid spreading, so that the liquid at the edge is detached from the large water droplet to move outward in the form of small water droplet with smaller diameters. At stage of the contraction phase, the spreading thickness of the droplet is small and the unevenness of the internal force causes it to break from the inside, so that the droplet crushes as a whole. It can be said that the first stage of the crushing occurs outside, while the second stage occurs internally.

Figure 17 shows the numerical simulation results of droplet crushing pattern at different times. When the impact velocity increases to a certain value, the surface tension of the droplet is insufficient to withstand the energy conversion caused by the kinetic energy of it; thus, the droplet fractures in the process of spreading on the surface. As can be seen from the diagram, when the droplet spreads to a certain diameter, the edge of it begins to tear by the initial regular circle. As the tearing degree increases, the liquid of the outermost ring of the droplet overcomes the intermolecular force and will break away from the main body and shrinks to a small droplet with a small diameter under the action of

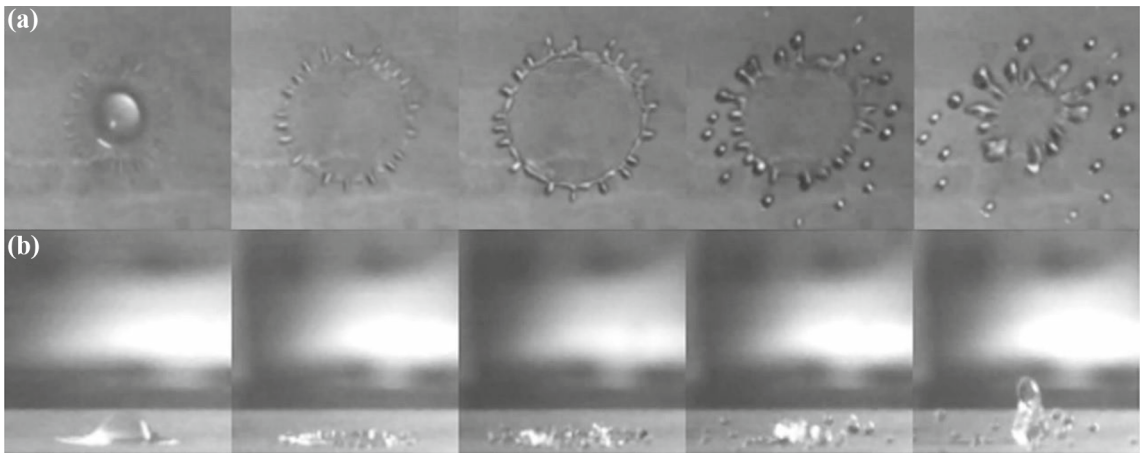

Fig. 16 The crushing fracture pattern of a droplet captured by a high-speed camera after it impacting on a superhydrophobic surface. **a** Top view of the droplet crushing process. **b** Front view of droplet crushing process

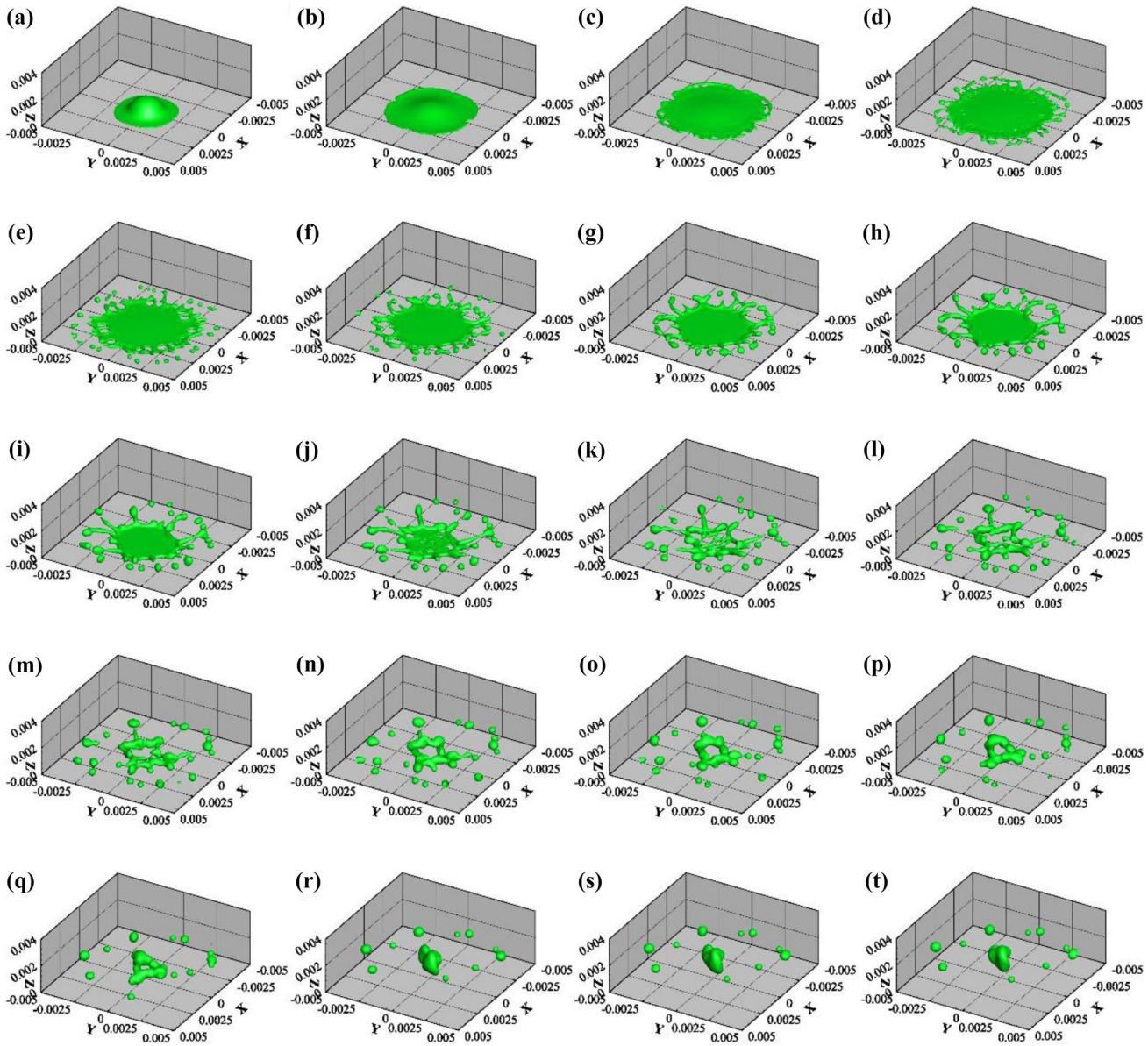

Fig. 17 The numerical simulation results of droplet crushing pattern at different times. **c–i** The droplet is gradually broken from the outer ring to the inner in layers, which includes the late stage of spreading and the early stage of contracting. **j–l** The droplet is gradually broken from the outer ring to the inner in layers, which includes the late stage of spreading and the early stage of contracting. **m–t** When the water droplets are completely broken, the force of the residual liquid in the central area will converge toward the center to form a small water droplet

surface tension and then continues to move outward under the action of inertia. While the intermolecular force of the internal liquid is greater than the inertia it receives, it is still connected to the main body of the droplet, thereby moving outward in the form of small branches. This stage is the first stage of fracture. The droplet is gradually broken from the outer ring to the inner in layers, which includes the late stage of spreading and the early stage of contracting (Fig. 17c–i). When the edge of the droplet is fractured, the spreading form of the main body of the droplet is extremely irregular, so that the liquid in the central area is unevenly distributed to generate dislocations, and finally, the droplet breaks from the inside. This stage is the second stage of fracturing, mainly in the middle and late stages of droplet contraction (Fig. 17j–l). When the water droplets are completely broken, the force of the residual liquid in the central area will converge toward the center to form a small water droplet (Fig. 17m–t). At this time, the surface energy of the droplet is converted into kinetic energy, so that the new water droplet contracts and rebounds at a large velocity.

Conclusion

In this paper, the dynamic process of the droplet impacting on a superhydrophobic surface is numerically simulated by the CLSVOF method. Through the analysis, the following main conclusions can be obtained:

1. The process of the droplet impacting on the surface can be summarized into four stages: falling, spreading, contracting and rebounding. Due to the difference in energy loss and force, the contracting process of the droplet on the surface is significantly longer than the spreading stage. In the contraction–rebound stage, the bottom of the droplet forms a concave "air cavity" due to the difference in velocity between the edge of the droplet and the central area.
2. In the whole process of the droplet impacting on the surface, the internal velocity and pressure of it are symmetrically distributed along the central axis. In the process of rebounding, the high-pressure zone is located at the top and bottom of the droplet, causing the droplet to rise in the form of constant retracting–stretching fluctuations
3. The crushing of the droplet is divided into two stages. The first stage occurs in the edge area of the droplet, which is mainly caused by surface tension; the second stage occurs in the inner area of the droplet, mainly due to uneven internal forces.

Acknowledgements This work was supported by Key Scientific and Technological Project of Jilin Province (Grant No. 20170204066GX), Science and Technology Projects in Jilin Province Department of Education (Grant No. JJKH20170785KJ and JJKH20180137KJ), The Advanced Manufacturing Projects of Government and University Co-construction Program funded by Jilin Province (Grant No. SXGJSF2017-2).

Compliance with ethical standards

Conflict of interest The authors declare no conflict of interest.

Ethical approval This review does not contain any studies with human or animal subjects performed by any of the authors.

References

1. Hsieh SS, Luo SY (2016) Droplet impact dynamics and transient heat transfer of a micro spray system for power electronics devices. Int J Heat Mass Transf 92:190–205
2. Piazzullo D, Costa M, Allocca L et al (2017) A 3D CFD simulation of GDI sprays accounting for heat transfer effects on wallfilm formation. SAE Int J Engines 10(4):2166–2175
3. Cossali GE, Marengo M, Santini M (2008) Thermally induced secondary drop atomisation by single drop impact onto heated surfaces. Int J Heat Fluid Flow 29(1):167–177
4. Kulju S, Riegger L, Koltay P et al (2018) Fluid flow simulations meet high-speed video: computer vision comparison of droplet dynamics. J Colloid Interface Sci 522:48
5. Fujimoto H, Oku Y, Ogihara T et al (2010) Hydrodynamics and boiling phenomena of water droplets impinging on hot solid. Int J Multiph Flow 36(8):620–642
6. Kim HY, Park SY, Min K (2003) Imaging the high-speed impact of microdrop on solid surface. Rev Sci Instrum 74(11):4930–4937
7. Yong CJ, Bhushan B (2008) Dynamic effects of bouncing water droplets on superhydrophobic surfaces. Langmuir ACS J Surf Colloids 24(12):6262–6269
8. Karapetsas G, Chamakos NT, Papathanasiou AG (2016) Efficient modelling of droplet dynamics on complex surfaces. J Phys Condens Matter 28(8):085101
9. Khojasteh D, Kazerooni NM, Salarian S et al (2016) Droplet impact on superhydrophobic surfaces: a review of recent developments. J Ind Eng Chem 42:1–14
10. Gauthier A, Symon S, Clanet C et al (2015) Water impacting on superhydrophobic macrotextures. Nat Commun 6:8001
11. Vafaei S, Podowski MZ (2005) Analysis of the relationship between liquid droplet size and contact angle. Adv Colloid Interface Sci 113(2–3):133–146
12. Vafaei S, Podowski MZ (2005) Theoretical analysis on the effect of liquid droplet geometry on contact angle. Nucl Eng Des 235(10–12):1293–1301
13. Zhang R, Hao PF, Zhang XW et al (2018) Supercooled water droplet impact on superhydrophobic surfaces with various roughness and temperature. Int J Heat Mass Transf 122:395–402
14. Lee D, Shin S (2018) Numerical analysis of impinging droplet on superhydrophobic cylindrical wall. J Comput Fluids Eng 23
15. Choi H, Shin S (2017) Numerical study of single droplet jumping on superhydrophobic surface with different initial contact conditions. J Comput Fluids Eng 22(4):109–115
16. Hao PF, Lv CJ, Niu FL et al (2014) Water droplet impact on superhydrophobic surfaces with microstructures and hierarchical roughness. Sci China Phys Mech Astron 57(7):1376–1381
17. Abolghasemibizaki M, McMasters RL, Mohammadi R (2018) Towards the shortest possible contact time: droplet impact on cylindrical superhydrophobic surfaces structured with macroscale features. J Colloid Interface Sci 521:17–23
18. Chu FQ, Yuan ZP, Zhang X (2018) Energy analysis of droplet jumping induced by multi-droplet coalescence: the influences of droplet number and droplet location. Int J Heat Mass Transf 121:315–320
19. Bordbar A, Taassob A, Khojasteh D et al (2018) Maximum spreading and rebound of a droplet impacting onto a spherical surface at low weber numbers. Langmuir 34(17):5149–5158
20. Sussman M, Puckett EG (2000) A coupled level set and volume-of-fluid method for computing 3D and axisymmetric incompressible two-phase flows. J Comput Phys 162(2):301–337
21. Son Gihun (2003) Efficient implementation of a coupled level-set and volume-of-fluid method for three-dimensional incompressible two-phase flows. Numer Heat Transf Part B Fundam 43(6):549–565
22. Hu H, Chen L, Huang S et al (2013) Breakup phenomenon of droplets impacting on a superhydrophobic brass surface. Tribology 33(5):449–455